JOURNAL OF PROPULSION AND POWER
Vol. 20, No. 3, May–June 2004

# Burning-Rate Predictor for Multi-Ingredient Propellants: Nitrate–Ester Propellants

Martin S. Miller* and William R. Anderson†
*U.S. Army Research Laboratory, Aberdeen Proving Ground, Maryland 21005*

**The theoretical capability to predict the burning rate of real propellants from their ingredients would be an invaluable aid to formulating new propellants. Despite progress over the last decade on a very few simple ingredients, such as cyclotrimethylenetrinitramine (RDX), and a few simple binary mixtures, no general capability of this sort exists today. This shortcoming is not due to insufficient computational resources, but to a lack of understanding of fundamental combustion mechanisms in the condensed phase and surface/gas interface for typical propellant ingredients and their mixtures. This difficult problem is likely to remain intractable for some time to come. It is demonstrated that our previously published semi-empirical formalism for single ingredients can be successfully extended to treat multi-ingredient propellants. In particular, the study is confined to nitrate–ester propellants (using M10, M2, M9, and JA2 as examples). However, the method should also be applicable to other classes of homogeneous propellants and even composite propellants where mixing of ingredients in a surface melt layer or sufficiently small particle sizes remove the multidimensional character. The method treats the gas-phase processes on the level of elementary reactions and multicomponent transport. A semi-empirical pyrolysis law coupled with informed estimates of the decomposition products of the condensed phase enables us to finesse the absence of knowledge of the detailed processes occurring in the condensed phase and at the burning surface. Results of a computer code, CYCLOPS, based on this approach, show that both the burning rate and flame structure are well predicted for a series of four U.S. Army gun propellants.**

## Nomenclature

$A_k$ = Arrhenius coefficient for $k$th reaction
$A_s$ = pyrolysis law coefficient
$c_p$ = specific heat capacity
$E$ = pyrolysis law activation energy
$h$ = enthalpy
$I$ = total number of propellant ingredients
$J$ = total number of different product species from all of the ingredients
$\dot{m}$ = mass flux
$N$ = total number of chemical species in all phases
$n_{\text{mon}}$ = number of nitrocellulose monomers in Monte Carlo simulation
$n_{ij}^{-0}$ = number of moles of product species $j$ produced by one mole of ingredient $i$ during surface decomposition
$\bar{n}_{\text{NO}_2}$ = average number of nitrate groups per monomer of nitrocellulose
$q(x)$ = volumetric heat release rate at $x$
$r$ = linear burning rate
$R$ = universal gas constant
$S_k$ = sensitivity of the temperature at some point to changes in the $k$th reaction coefficient
$T$ = temperature
$T_2$ = temperature at the second grid point in the numerical calculation of gas-phase flame
$V$ = molar volume of pure ingredient
$W$ = molecular weight
$\bar{W}_{\text{NC}}$ = average molecular weight of a nitrocellulose specimen
$X$ = mole fraction
$x$ = spatial coordinate normal to burning surface
$Y$ = mass fraction
$\lambda$ = thermal conductivity
$\rho$ = mass density
$\sigma_p$ = temperature sensitivity
%N = percent atomic nitrogen by weight

*Subscripts*

av = average
C = carbon atom
$g$ = gas phase
H = hydrogen atom
$i$ = chemical species $i$
$j$ = chemical species $j$
$k$ = chemical species $k$
$m$ = maximum value in calculational domain
mon = monomer
N = nitrogen atom
NC = nitrocellulose
O = oxygen atom
$s$ = propellant surface

*Superscripts*

$-0$ = quantity at the condensed-phase side of the propellant surface
$+0$ = quantity at the gas-phase side of the propellant surface
$-\infty$ = quantity at the infinite boundary of the unreacted propellant at initial temperature

Received 4 November 2002; revision received 1 August 2003; accepted for publication 16 September 2003. This material is declared a work of the U.S. Government and is not subject to copyright protection in the United States. Copies of this paper may be made for personal or internal use, on condition that the copier pay the $10.00 per-copy fee to the Copyright Clearance Center, Inc., 222 Rosewood Drive, Danvers, MA 01923; include the code 0748-4658/04 $10.00 in correspondence with the CCC.

*Research Physicist, Propulsion Science Branch.
†Research Chemist, Propulsion Science Branch.

## I. Introduction

THE trial-and-error approach has always played a central role in the development of new energetic materials for use as explosives and propellants. It is an approach dictated by necessity, not by choice. Final service acceptance of a new propellant has historically required extensive small- and large-scale testing involving enormous monetary resources, lengthy development times, and the generation of great amounts of hazardous waste both in the manufacture of failed formulations and in their disposal. These burdens have been exacerbated over the last few decades by a number of other factors. The increasing sophistication of weapons systems has

meant that their overall cost has grown far beyond that of the raw energetic materials that they utilize. Moreover, the escalating level of performance of these weapons systems has resulted in diminishing margins for error with regard to their proper functioning and safe operation. The combination of these new fiscal, temporal, environmental, and safety constraints make it imperative that future propellant-development programs reduce their reliance on the inefficient and wasteful trial-and-error method. The most rational way to accomplish this goal is through the development of smart, computational design tools derived from a sound scientific understanding of propellant combustion.[1]

Unfortunately, in the field of propellant combustion, the laws of nature are not readily revealed. In part this is due to the extremely hostile environment that propellants generate. In large guns, for example, action times range from a few tens of milliseconds for tank cannon to a few hundreds of milliseconds for an artillery piece. In this short time, the solid propellant is transformed from a metastable state at ambient temperature to equilibrium products at several thousands of Kelvins and pressures up to 7000 atm. The reaction zone critical to determining the burning rate extends a mere hundred micrometers from the surface even at 10 atm and diminishes at higher pressures. Spatial temperature gradients at the burning surface are of the order of 10,000 K/cm at 10 atm and increase at higher pressures. Conducting controlled experiments under any one of these harsh circumstances of eye-blink times, hair-width distances, refractory temperatures, and crushing pressures presents a considerable experimental challenge, but the simultaneous presence of all four creates almost insuperable obstacles. Even under constant-pressure conditions, propellant flames are flickering by nature, which compounds the other experimental difficulties. In addition to such macro-scale difficulties, the underlying mechanism of propellant combustion involves significant condensed-phase reactions and hundreds of gas-phase reactions among many dozens of species. The rates of most of these reactions are sensitive to both temperature and pressure. The result is an impressive tangle of physical and chemical phenomena.

Notwithstanding all of the difficulties, progress in the basic science of propellant combustion has been achieved over the last dozen years. The major gas-phase chemical species and some radicals have been measured in flames of a number of burning energetic materials and propellants. Computational models have been developed that treat, with a high degree of rigor, the gas-phase processes, including reactions, convection, molecular diffusion, and thermal conduction. The condensed-phase treatment in these models is limited, not (so far) by computational insufficiency, but by the lack of definitive experiments revealing the detailed nature of the physical and chemical processes occurring there. A number of credible gas-phase reaction mechanisms have been assembled appropriate to several energetic compounds, and although some details of these mechanisms still require further study, the greatest speculation embodied in the models, by far, is in the detailed description of the condensed phases. Whereas reliable experimental and theoretical methods are well established to refine our understanding of the gas-phase processes, such is not the case for the condensed phase. Unfortunately, because of nearly intractable experimental and computational difficulties, this condition is not likely to be remedied in the near future.

To overcome this impasse, we recently proposed a hybrid approach[2] in which the conversion of condensed-phase material to gas is described by a semi-empirical relation, known in the propellant literature as a pyrolysis law, and the gas-phase processes of reactions and transport are described in elementary-reaction detail with considerable rigor. In this paper, we extend this approach to include multi-ingredient propellants and illustrate its promise through application of the model to several actual gun propellants. Our calculations of burning rate for real nitrate–ester-base propellants, including the complex ingredient nitrocellulose, are the first to be based on elementary reactions in the gas phase. It is expected that the proposed model will be useful for other classes of ingredients as well. In fact, we believe that the hybrid-rigor paradigm developed will provide the best quantitative description of propellant burning rate (and the gas-phase effects of modifiers on burning rate) for many years to come, possibly to be supplanted by molecular-dynamics descriptions of detailed condensed- and interphase processes. The multi-ingredient model has been formalized into a computer code called CYCLOPS. It is hoped that it will play a role in developing the next generation of high-performance gun propellants.

## II. Single-Ingredient Model

A key objective in the modeling of energetic-material combustion is the development of a mathematical description of the transformation of an ambient-temperature energetic solid in stable chemical disequilibrium into a high-temperature, multicomponent gas at equilibrium. This transformation involves a considerable complexity of physical and chemical processes. The energetic material may decompose in the condensed phase, may undergo considerable reaction there, and may form a liquid layer at the burning surface. Gases may be evolved from these subsurface reactions and either dissolve in the liquid, or form bubbles, or both. At the surface, gases may be produced by reaction, or evaporation, or both. In general, many reactive species are formed at or near the surface. There they undergo a complex sequence of reactions influenced by the transport of heat and species from one part of the flame to another by convection, diffusion, and thermal conduction. As already stated, our knowledge of the chemical and physical processes in the condensed phase is scant. Furthermore, methods to elucidate these processes with reliability have yet to be developed. Our understanding of and ability to describe the transport processes and reactions in the gas phase, on the other hand, is quite highly developed. In the gas phase, even if a particular reaction's rate and its products are uncertain, the means to measure or calculate these data to greater precision are, for the most part, available. Unfortunately, our ignorance of the condensed-phase processes deprives us even of the types and numbers of chemical species emerging from the surface and their rates of emergence, that is, critical boundary conditions required for the sophisticated gas-phase calculations. Eventually reactive molecular-dynamics calculations may supply the necessary condensed-phase descriptions, but given the primitive state of reactive force fields at present, we believe that time is many years away.

Our interim solution[2] to this dilemma was to estimate the identities and mole fractions of species emerging from the condensed phase and to describe their mass rate of emergence by the conventional pyrolysis-law formalism. Because the pyrolysis law must, at present, be measured, such a strategy would effectively be useless if a pyrolysis law must be measured for every ingredient and combination of ingredients. After decades of work, Zenin[3] has shown that double-base (DB) propellants with nitroglycerine (NG) components ranging from 0 to 50% and nitrocellulose (NC) of percent nitrogen ranging from 11.5 to 13.5% by mass can all be described by a universal pyrolysis law. Furthermore, this same law holds for DB propellants with cyclotetramethylenetetranitramine (HMX) and various catalytic additions. This remarkable finding motivated the hybrid-rigoro approach described earlier. The resulting model was shown to provide good results for the burning rate of frozen ozone, NG, and cyclotrimethylenetrinitramine (RDX) (Ref. 2). The tantalizing possibility of using the approach as a formulation aid was also demonstrated by the first application of a detailed-chemistry energetic-material model to binary mixtures of NG with a few simple molecular additives.

A mathematical derivation of the basic model and its relation to previous work is given in detail elsewhere[2]; however, a brief summary of the key relationships will be given here to aid the continuity of development. The model treats two computational domains, the condensed phase and the gas phase. In the condensed phase, two key assumptions are made: In-depth reactions are negligible, and molecular diffusion is negligible. These assumptions enable a derivation of the energy-flux boundary condition at the surface in the following form[2]

$$\lambda_g \left( \frac{\mathrm{d}T}{\mathrm{d}x} \right)^{+0} = \dot{m} \sum_{i}^{N} \left( Y_i^{-0} h_i^{+0} - Y_i^{-\infty} h_i^{-\infty} \right) \tag{1}$$

The set of mass fractions $\{Y_i^{-0}\}$ defines the distribution of gas-phase species we assume evolve from the condensed phase, which in this

work is assumed to be independent of pressure, whereas the set $\{Y_i^{-\infty}\}$ is simply the propellant-ingredient mass fractions. Thus, the term on the right side of Eq. (1) represents the heat required to change the propellant ingredients (in their initial state) to our assumed condensed-phase product distribution (in the gaseous state), and the quantity on the left side of the same equation is, of course, the heat feedback from the gas-phase reaction zones. Note also that this version of the boundary condition has the very great advantage of requiring only the enthalpy of the starting material at the initial temperature and only the enthalpies of the condensed-phase decomposition products *in the gas state* at the surface temperature. Thus, the highly uncertain thermochemical and thermophysical properties of the expanding and possibly melting condensed phase near the surface are not needed. The price of this reduction in required data is that the model cannot compute the temperature profile through the condensed phase(s), except under the further assumption of constant thermal properties there. This compromise, however, is not a serious limitation to our goals.

In the two-phase steady-state combustion problem, there are normally two eigenvalues, the mass flux $\dot{m}$ and the surface temperature $T_s$. In the present model, the number is reduced to only one eigenvalue, conveniently taken as $\dot{m}$, by virtue of the semi-empirical pyrolysis-law relationship

$$\dot{m} = A_s \exp(-E_s/RT_s) \tag{2}$$

The solution proceeds, then, by providing a starting guess for $\dot{m}$ and computing the corresponding surface temperature from Eq. (2). This defines the equivalent of a burner-stabilized flame problem with elementary reactions. We modified the PREMIX code[4] to solve the gas-phase conservation equations. CYCLOPS calls this modified code as a subroutine. The gas-phase solution then determines the heat feedback to the surface [left side of Eq. (1)]. Note, because the length of the computational domain (the keyword XEND in PREMIX) can affect the heat feedback, the CYCLOPS code automatically extends this domain until successive computations of the heat feedback differ by no more than 0.1%. The results are checked to see if the surface energy-flux boundary condition [Eq. (1)] is satisfied. If not, a new value of $\dot{m}$ is chosen by an algorithm, and the whole procedure iterated until the eigenvalue is found to an accuracy of 1%. The algorithm employs a modified secant method to locate coarsely the eigenvalue first; then the root is automatically refined by the bisection method to establish absolute conformance of the eigenvalue to the 1% criterion. Experience indicates that these criteria provide burning rates that are numerically accurate to within a few percent.

Note that the success of the single-ingredient model depends largely on getting three inputs right: the pyrolysis law, the net condensed-phase decomposition products, and the gas-phase reaction mechanism. [Other data, such as the heats of formation of the ingredients, may also play a significant role (discussed later).] The pyrolysis law may, in principle, be obtained either by theoretical or experimental means. An example of the theoretical path was given previously[2] for the case of frozen-ozone deflagration. In that case, a law in the form of Eq. (2) was fit to detailed calculations of an evaporation surface-regression mechanism. For more complex energetic materials, measurements of the pyrolysis law are generally required. As for the (nonequilibrium) decomposition products of the condensed phase, so long as there is a sharply defined surface boundary, one can say that there will exist some such set of decomposition products at the surface of every deflagrating energetic material. We may not be able to discern easily what this set is, but at least the concept that such a set exists is sound. The implicit assumption that the products of the condensed-phase decomposition do not change with pressure is harder to justify. Without pressing the point too vigorously, nonetheless, note that the burning rate of most propellants varies over many decades of pressure as a power law in pressure. This same dependence arises from overall-reaction models, which also have reactants unchanging with pressure.[5] Such an argument is admittedly inferential, but it is suggestive that the assumption of pressure-independent surface products may not be inappropriate to the propellant problem. In any case, the mathematics of the model developed here do not depend on the assumption that the condensed-phase product set is independent of pressure; if known, changes in the product set with pressure could easily be included.

Finally, although a given gas-phase reaction mechanism may be imperfect, there exist theoretical and experimental techniques to improve the description of practically any elementary reaction, given sufficient resources. Thus, a successful calculation of burning rate using this model must be possible even if the detailed condensed-phase processes are not known, provided that accurate information for the mentioned inputs can be found. Therefore, the model should be a durable and versatile framework for quantitatively incorporating new research results on the detailed processes of propellant combustion.

The semi-empirical approach taken here, requiring as it does estimates of the chemical products of the condensed-phase reactions, may appear to be less rigorous and more speculative than models that hypothesize specific reaction paths in the condensed phase and compute their effects explicitly. On the contrary, we believe that those models that treat the condensed-phase processes explicitly are far more speculative than what we have proposed, given the current impoverished state of knowledge of those processes. In those models not only must surface gasification mechanisms and specific reaction paths be hypothesized, but also the reaction rate parameters must be estimated. This argument was posited in greater detail previously.[2]

## III. Multi-Ingredient Model

A practical solid propellant is almost always a mixture of ingredients. This poses a number of new problems beyond those inherent in the single-ingredient model. One such problem is the issue of determining the total starting-material enthalpy. Enthalpies of solution and mixing logically should be included, so that the enthalpy of the propellant is not simply the sum of the enthalpies of the ingredients as assumed in the derivation of Eq. (1). In practice, however, such refinements are not normally considered in thermochemical-equilibrium calculations for propellants. This neglect is, for the most part, due to the unavailability of these interaction energies, although some justification may be found in that such energies are generally relatively small corrections to the sum of the ingredient enthalpies. Molecular dynamics calculations may some day be routine in computing the total enthalpy of the propellant amalgam; however, for the present we follow the expedient convention of summing the ingredient enthalpies. Note, however, that these effects may not always be insignificant. In computing the enhancement of the linear burning rate of NG by adding a small amount (2.4% by weight) of $NH_3$, we previously found[2] that using the gaseous-state enthalpy for $NH_3$ results in a 19% burning rate boost, whereas using the liquid-state enthalpy of $NH_3$ produced only a 12% boost. The reason is that more of the gas-phase heat feedback is wasted in supplying the latent heat of vaporization in the latter case. Enthalpies of solution or mixing are presumably closer in magnitude to enthalpies of fusion than to enthalpies of vaporization, so that the effect should be generally smaller than suggested by this example; nevertheless, note that the propellant enthalpy is presently only approximated and that the effect of this approximation on the burning rate is not readily assessed.

Another issue that arises in the multi-ingredient model involves the net gaseous decomposition products evolving from the condensed phase of the propellant mixture. There is the distinct possibility that, during reactive condensed-phase decomposition, the products evolving from the mixture may not be the same as those from the noninteracting component ingredients. This may happen either because the presence of one ingredient may alter the course of decomposition of another ingredient or because of reactions between the ingredient products in the condensed phase. In this work, however, we assume that no such interactions occur, that is, that the propellant decomposition-product mole fractions may be computed from the decomposition products of each ingredient according to the proportion of each ingredient in the propellant. As with the

mixture enthalpy problem just discussed, there is little recourse to this approach at the present time. Unlike the mixture enthalpy problem, however, we have little evidence for believing this procedure to be a good approximation. On the other hand, in the absence of further understanding about the condensed-phase reactions, this approach is certainly reasonable and least biased in an a priori sense. Its justification must come largely from whatever success the model enjoys by its employment. It may well turn out that the assumption of noninteractive decomposition works well for some combinations of ingredients but not for others.

The net mole fractions of condensed-phase products arising from the propellant mixture is, therefore, calculated as follows. Suppose that one mole of ingredient $i$ produces $n_{ij}^{-0}$ moles of condensed-phase product species $j$. Then the net mole fraction $X_k^{-0}$ of product species $k$ on the condensed-phase side of the surface arising from all ingredients is given by

$$X_k^{-0} = \frac{\sum_i^I \left[\left(Y_i^{-\infty}/W_i\right) n_{ik}^{-0}\right]}{\sum_j^J \sum_i^I \left[\left(Y_i^{-\infty}/W_i\right) n_{ij}^{-0}\right]} \tag{3}$$

The set of mole fractions $\{X_k^{-0}\}$ are the boundary conditions required for solution of the gas-phase species-conservation equations. In words, we find a set of decomposition products that leads to a reasonably good computed burning rate for each ingredient, then compute by Eq. (3) the net mole fractions of each surface product produced by all of the ingredients, properly weighted by the relative amounts of the ingredients that make up the propellant.

Mass density of the propellant mixture is computed by the simple method of additive partial molar volumes as described in Ref. 2 and given by

$$\rho_{\text{mix}} = \frac{W_{\text{av}}}{\sum_i X_i V_i} \tag{4}$$

This approximation assumes negligible distortion of the pure-ingredient molar volumes by the dissimilar-molecule interactions. It is the best approach one can take short of molecular-dynamic simulations for each case. (See the end of the next section for additional discussion.)

The accuracy of the multi-ingredient model will naturally depend (at best) on the accuracy with which the model reproduces the burning rates of the pure ingredients. Rather than this being a disadvantage, we expect that the predicted burning rate of the multi-ingredient model will be somewhat forgiving of inaccuracies in any single ingredient simply because the overall degree of integration is higher. It is well known among combustion modelers that often the burning rate is surprisingly insensitive to the details of the underlying processes; it is hoped that this experience will work to our advantage in the multi-ingredient model.

## IV. NC, Special-Case Ingredient

NC is a major ingredient in conventional smokeless propellants. It is also an ingredient presenting formidable complexity to the modeler. NC exists as a long-chain polymer with three potential nitration sites on each monomer. The monomer with all sites nitrated, cellulose trinitrate, is shown in Fig. 1. The three carbon-atom nitration sites are labeled 2, 3, and 6. If at one or two of these sites the O–$NO_2$ group is replaced by an hydroxyl group, the resulting monomers

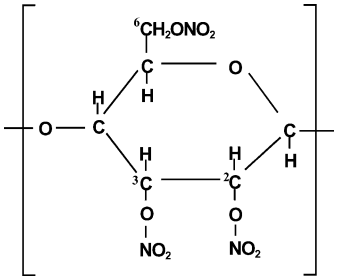


**Fig. 1 Schematic of cellulose trinitrate monomer.**

are referred to as cellulose dinitrate and cellulose mononitrate, respectively. A given specimen of NC is characterized by an average nitration level expressed as the percent of nitrogen-atom mass to average monomer mass. The average percent nitrogen, %N, is related to the average number of nitrate groups per monomer, $\bar{n}_{NO_2}$, by the definition

$$\%\text{N}/100 \equiv \bar{n}_{NO_2} W_{\text{N}}/\bar{W}_{\text{NC}} \tag{5}$$

From this relation one can determine that the percent nitrogen corresponding to the pure mononitrate is 6.76%, to the pure dinitrate is 11.11%, and to the pure trinitrate is 14.14%.

Because military NC is typically in the range of 12–13 %N, one might at first suppose that it consists of a mixture of only di- and trinitrates, but this is not the case. Leider and Seaton[6] have investigated the distribution of nitration states, that is, the fractions of mononitrates, dinitrates, and trinitrates, for an NC specimen of given average percent nitrogen. They performed Monte Carlo calculations for two cases, which depended on different assumptions as to the probability of nitration at given sites. In one case, nitration at sites 2, 3, and 6 were considered equally probable, which results in some monomers being unnitrated, and in the other, they assumed at least one site was always nitrated. Their assumed nitration level corresponded to 12.15 %N, which was chosen to match their test specimens. They also examined the case of at least two sites being nitrated; this case can be done analytically. The case that best fit their thermal-decomposition experiments, involving weight loss and gas evolution, was the one where at least one site was always nitrated.

Using the findings of Leider and Seaton,[6] we developed our own Monte Carlo code to determine the distribution of nitrate states for a given value of average percent nitrogen. We assume that, for military NC, at least one site is nitrated and that C6 is the preferred site. This choice is consistent with the isotope-substitution work of Gelernter et al.,[7] who established that the nitrate group at the C6 position is the most stable. The remaining sites, C2 and C3, are considered equally probable for nitration. The assumption that C6 is the most stable while C2 and C3 are equally probable is also supported by quantum-mechanical structure calculations.[8] The Monte Carlo code, a subroutine of CYCLOPS, works as follows. First, the given percent nitrogen is converted to the average number of $NO_2$ groups per monomer, $\bar{n}_{NO_2}$,

$$\bar{n}_{NO_2} = \frac{[(\%\text{N}/100)(6W_{\text{C}} + 10W_{\text{H}} + 5W_{\text{O}})]}{[W_{\text{N}} - (\%\text{N}/100)(W_{\text{N}} + 2W_{\text{O}} - W_{\text{H}})]} \tag{6}$$

This relation follows after a little algebra from Eq. (5). One then considers an NC system consisting of $n_{\text{mon}}$ monomers. Because for mititary NC we assume that the C6 position is always occupied by an $NO_2$ group, $n_{\text{mon}}(\bar{n}_{NO_2} - 1)$ is the number of excess $NO_2$ groups to be distributed among the $(2n_{\text{mon}})$ available C2 and C3 sites in the NC system. In the Monte Carlo description, no distinction is made between dinitrates with C2 occupied by an $NO_2$ group and those with C3 occupied (although we have hypothesized that the decomposition product sets are different). This distribution is done randomly, and the result defines one system configuration. The process is repeated for many configurations and the distribution fractions compiled as averages over all of the configurations. Experimentation showed that a system consisting of 1000 monomers and 1000 configurations was sufficient to maintain two-place precision in the distribution fractions, and such precision was considered commensurate with that of other data used in the burning-rate calculation. Figure 2 shows how the distribution among nitrate states varies with the given percent nitrogen according to this model.

Recent experimental work allows a more direct test of the Monte Carlo model predictions than did the experiments performed by Leider and Seaton.[6] Todd and Glasser[9] used nuclear magnetic resonance (NMR) spectroscopy to determine the distribution of nitrate groups in the nitrocellulose repeat units, or what we have more loosely termed the NC monomers. Their data for NC specimens of two different nitration levels and several blend samples of the same percent nitrogen are shown along with our Monte Carlo model predictions

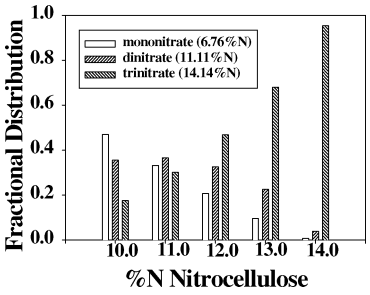


**Fig. 2 Nitrate-state distribution according to the Monte Carlo code.**

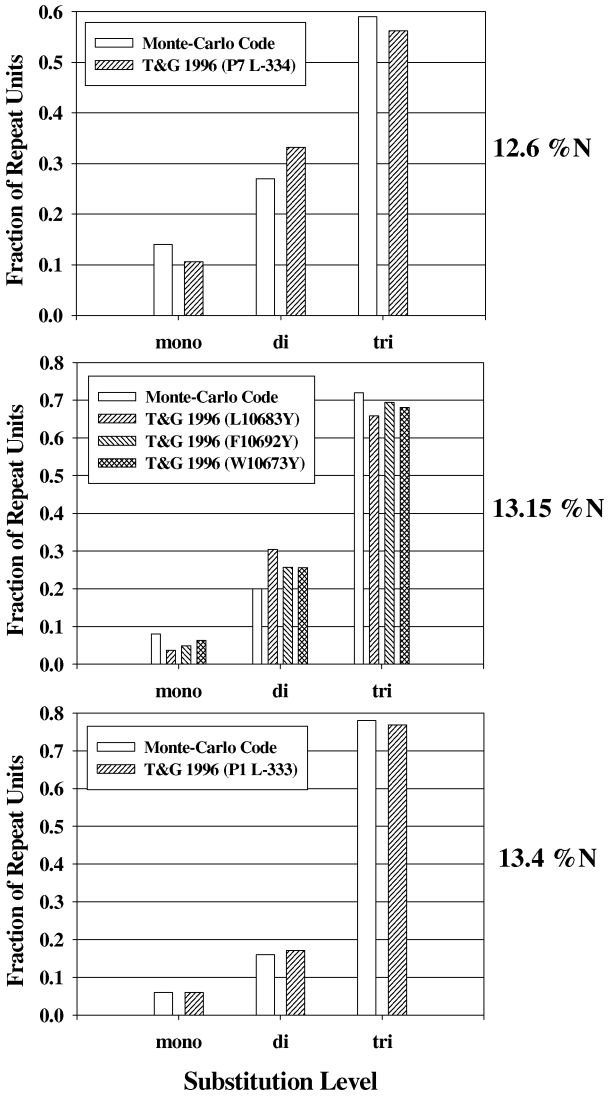


**Fig. 3 Comparison of Monte Carlo code predictions of nitrate-state distributions to NMR measurements of Todd and Glasser.[9]**

in Fig. 3. It can be seen that the model simulates the distribution with uncertainties that are of the order of the measured variations, which are due both to experimental errors and possibly to variances in the homogeneity of the NC samples themselves.

With the Monte Carlo model in hand, NC as a propellant ingredient is treated in the burning rate model as comprising three separate ingredients: cellulose mono-, di-, and trinitrate. One must provide properties and a set of decomposition products for each of these substituents in the ingredient database (discussed in the next section). The heats of formation (on a per-mole basis) of the different states of nitration of NC are obtained from a second-degree-polynomial fit (shown in Fig. 4) to data derived from the per-gram heat-of-formation expression reported by Taylor et al.[10] The mass densities of each of the nitration states are required as well; these were

**Table 1 Weight percents of propellant ingredients according to nominal specifications: actual/code-assumed**

| | Propellant | | | |
|---|---|---|---|---|
| Ingredient | M10 | M2 | M9 | JA2 |
| NC | 98.0/100 | 77.45/79.9 | 57.75/59.1 | 59.50/60.0 |
| %N | 13.15 | 13.25 | 13.25 | 13.1 |
| NG | —— | 19.50/20.1 | 40.0/40.9 | 14.90/15.0 |
| DEGDN | —— | —— | —— | 24.80/25.0 |
| DPA | 1.0/0 | —— | —— | —— |
| EC | —— | 0.60/0 | 0.75/0 | —— |
| KNO3 | —— | 2.15/0 | 1.50/0 | —— |
| KSO4 | 1.0/0 | —— | —— | —— |
| Graphite | —— | 0.30/0 | —— | 0.05/0 |
| MgO | —— | —— | —— | 0.05/0 |
| Akardit II | —— | —— | —— | 0.70/0 |

**Table 2 Comparison of measured[11] propellant densities and present predictions using Eq. (4)**

| Propellant | Predicted density, g/cm$^3$ | Measured density, g/cm$^3$ | %Error |
|---|---|---|---|
| M10 | 1.638 | $1.51 \pm 0.01$ | 8.5 |
| M2 | 1.630 | —— | —— |
| M9 | 1.620 | $1.62 \pm 0.02$ | 0 |
| JA2 | 1.558 | $1.57 \pm 0.01$ | −0.8 |

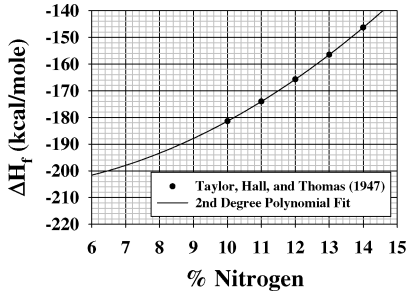


**Fig. 4 Heats of formation of NC as a function of % N generated as an analytic fit to the measurements of Taylor et al.[10]**

obtained by molecular-dynamic simulations of the homopolymers using the COMPASS force field.[8] The results are cellulose mononitrate $\rho = 1.5250$ g/cm$^3$, cellulose dinitrate $\rho = 1.5778$ g/cm$^3$, and cellulose trinitrate $\rho = 1.6640$ g/cm$^3$.

Using these homopolymer densities, the measured densities of other ingredients, and the code-assumed propellant formulations given in Table 1, we compare the values predicted by Eq. (4) to measured propellant densities[11] in Table 2. The densities are predicted to within about 1% in all cases except M10. Being a single-base propellant, M10 is poorly plasticized and may well include voids created during the drying process; this would cause a prediction error in the direction seen. Accurate prediction of the density for such propellants may require a molecular-dynamic simulation that accounts for the migration of solvent from the molecular interstices during drying.

## V. Ingredient Database: Work in Progress

Though vastly more complex, the CYCLOPS code works much like a thermochemical equilibrium code in that it reads an input file containing the name of the propellant, the names and weight fractions of each of the ingredients, the initial temperature, and the pressure for which the burning rate is desired. If a propellant includes NC as one of its ingredients, an input value of the percent nitrogen is also required; in that event, a call is then made to the Monte Carlo subroutine, which returns the molar fractions of mono-, di-, and trinitrates. The properties of each ingredient, including molecular weight, mass density, specific heat, heat of formation, and condensed-phase decomposition products, reside in an

ingredient database file, which is read as required by the CYCLOPS code.

At the present time there is no way to remove an element of speculation in setting down the condensed-phase decomposition products evolving from the surface from each ingredient, and so it is to be expected that the ingredient database will be a work in progress, being refined as experience, new experiments, or theory suggests better choices. The only conservation principle constraining the choice of these decomposition products is elemental balance in writing the overall chemical reaction from unreacted compound to products. Beyond that, for guidance one might appeal to thermal-decomposition experiments, although awareness of the possible role of heating rate and secondary reactions may limit the suitability of many of these experiments. Also, one might argue by analogy with reaction paths for known reactants or reactant subgroups, or, even more crudely, base arguments on average bond energies. Finally, one is constrained by the practical requirement that the reaction mechanism must include any proposed decomposition species, although the mechanism certainly may be expanded, with varying degrees of difficulty, to include new species as required. Of course, an obvious criterion is the degree to which use of a particular set of ingredient products leads to a calculated burning rate that agrees with experiment. Use of this last criterion presupposes a high level of confidence in the pyrolysis law and gas-phase reaction mechanism. Variation of the burning rate with different condensed-phase decomposition-product sets was illustrated previously for NG (Ref. 2).

Ideally, the best set of decomposition products to use for a given ingredient would be determined by computing the burning rate for the neat ingredient based on many possible sets and accepting the one that is both theoretically sound and leads to the best agreement with experimental burning rates. Several circumstances can interfere with this approach. Experimental burning rate data may not be available for some ingredients, or, as in the case of each nitration state of NC being considered a separate ingredient, it may not even be possible to prepare a pure form of the ingredient for experimental test. Some secondary energetic ingredients burn much more slowly than the main energetic ingredients and prove to be troublesome with regard to achieving convergence in the PREMIX code. Finally, some ingredients, such as inert binders, will not undergo self-sustained combustion at all. In all of these cases, one simply has to do the best one can and be open to improvements. For example, cellulose trinitrate has a %N of 14.14%, but the most similar material for which we have burning rates is M10 propellant with a %N of 13.15% (Table 1.) Therefore, we expect that cellulose trinitrate will have a burning rate somewhat higher than M10. We investigated about two dozen different condensed-phase decomposition sets for cellulose trinitate, most of which led to burning rates much above or much below the experimental burning rate of M10, which is a mixture of nitration states. We selected the set that produced burning rates somewhat above that of M10, allowing for the energy-diluting effects of the lower nitrate states in the propellant compared to a pure cellulose nitrate. Our universe of tested decomposition sets was not (probably could not have been) comprehensive; there may well exist a better choice. The one selected, however, does result in reasonable agreement for the range of propellants examined. The decomposition sets for the dinitrate and the mononitrate were then selected by analogy with the decomposition scheme of the trinitrate. Note that, once a set of decomposition products is established for a particular ingredient, that set is fixed for all propellant formulations using the ingredient. This is the source of our claim for predictability. Also note the decomposition sets for some ingredients are assumed to include radicals, for example, H, HCO, and $CH_3$. It has proven necessary to do this to obtain agreement with experimental burning rates and flame structures. Radicals have not been observed in propellant and ingredient decomposition experiments. However, due to their high reactivities, radicals could not survive in such experiments. Therefore, the lack of observation of these, and perhaps other, species does not preclude the possibility of their importance in the initially evolved gas-phase mixture.

The ingredient database used for the calculations reported in this paper is given in Appendix A. The net mole fractions of the decomposition products from each of the propellants, resulting from the decomposition of each of their respective ingredients, are collected in Table 3. Values for heats of formation for all of the ingredients except for NC were taken from the Hunter thermochemical equilibrium code.[12,13] Where more than one value for an ingredient is given in the Hunter database, we used the average value.

**Table 3 Summary of computed net mole fractions of condensed-phase decomposition products**

| Decomposition product | Propellant | | | |
|---|---|---|---|---|
| | M10 | M2 | M9 | JA2 |
| NO2 | 0.2930 | 0.3204 | 0.3466 | 0.2771 |
| HONO | —— | 0.0115 | 0.0243 | 0.0579 |
| CHOCHO | —— | —— | —— | 0.0211 |
| HCO | 0.1111 | 0.1092 | 0.1071 | 0.1050 |
| CH2O | 0.2222 | 0.2414 | 0.2627 | 0.2415 |
| CH2 | 0.1111 | 0.0919 | 0.0706 | 0.0919 |
| CH3 | —— | —— | —— | 0.0140 |
| CH4 | —— | —— | —— | 0.0070 |
| CO | 0.2222 | 0.1954 | 0.1655 | 0.1574 |
| H | 0.0404 | 0.0302 | 0.0232 | 0.0271 |

## VI. Gas-Phase Reaction Mechanism: Work in Progress

The gas-phase reaction mechanism is much more solidly based in experiments and theory than are the suppositions as to the condensed-phase decomposition products; yet, like the ingredient database, it also must be considered a work in progress. New information on heats of formation, specific heats, reaction rates, and products of elementary reactions are continually becoming available, requiring periodic updates in the reaction mechanism. Because our present reaction mechanism comprises 59 chemical species and 365 reversible reactions, it can readily be appreciated that updating both the reaction mechanism and all of the consequent burning-rate calculations is not a trivial exercise. The reaction mechanism utilized for the present calculations is provided in Appendix B. It is to be expected that updates to the reaction mechanism may well result in poorer agreement between the predicted burning rates and experimental ones. One might then have to modify the decomposition products to recover acceptable agreement between predicted and theoretical burning rates.

The present mechanism is much larger than the one used for our single-ingredient calculations.[2] Like the previously used mechanism, the present one started from a version of our dark zone mechanism.[14–17] In the previous work,[2] we attempted to pare down the number of reactions, primarily by intuitive guesses that certain species might not matter rather than by actual comparative calculations. The reason for this approach was that the computational resources available were being strained to their limits. Since that time, computational resources have improved. We now find that some of the reactions left out are, in fact, important. In particular, we had deleted 10 species, HCN, HNCO, HOCN, HCNO, CN, $H_2CN$, $C_2N_2$, HNC, NCNO, and NCN, and about 70 reactions that describe the HCN/HNCO chemistry. (Note that NCO was included in the previous mechanism.) At the time we thought that these deleted species and reactions were only likely to matter for nitramine ingredients, but it turns out they are formed in trace amounts and are important in the dark zones of nitrate esters. (See subsequent discussion in Sec. IX.) Another major change from the dark zone mechanism is the addition of many reactions pertinent to $CH_4/O_2$ combustion taken from the Gas Research Institute consortium mechanism 2.11.[‡] These are denoted by the symbols <=> replacing = in Appendix B.

Additionally, we now find that two HCO + HCO reactions producing different product sets (R355 and R356, where R355 means reaction 355 in Appendix B) are very important. Because our

[‡]Available online, Bowman, C. T., Hanson, R. K., Davidson, D. F., Gardiner, W. C., Jr., Lissianski, G. P., Smith, G. P., Golden, D. M., Frenklach, M., and Goldenberg, M., GRI Mech, Ver. 2.11, at http://www.me.berkeley.edu/gri_mech/ (February 1997).

previous[2] product set for the single ingredient NG included HCO, leading to a high concentration of this species in the near-surface region, we suspected inclusion of these reactions might lead to a big change in predicted NG burning rates. Indeed, it does cause predicted rates to increase strongly, due to increased near-surface heat release, necessitating a change in assumed surface products for that ingredient (Appendix A).

Another major difference is that chemistry of ketene ($CH_2CO$) and glyoxal (CHOCHO) has been included. It was thought these species might actually play a role as surface products; thus, they were tried as such for several of the trial ingredients. Although only the latter species is retained as an assumed surface product [for diethyleneglycol dinitrate (DEGDN)], ketene formation near the surface is very important because $CH_2 + CO + M = CH_2CO + M$ ($-$R358, which means the reverse of R358) is very important for near-surface heat release and, consequently, for the heat feedback.

Finally, the last major change is that the rate coefficient of R19, $HNO + NO = N_2O + OH$, has been increased by a factor of two. It has long been known that calculations of dark zone structure are highly sensitive to this reaction, especially for nitrate ester propellants.[14–17] The rate coefficient previously used was obtained from the excellent review by Diau et al.,[18] in which they analyzed their group's own new experimental data, and all prior data from static reactor experiments on $H_2$/NO mixtures. (See quoted references in Ref. 18.) Unfortunately, in the analysis, they used an ancillary datum for the heat of formation of HNO, which is now known to be in error.[19] In unpublished work, Anderson has shown that calculations for the $H_2$/NO mixtures and for propellant dark zone length are very sensitive to this heat of formation. The reason is that R3 and R161, which strongly influence the [HNO], have nonnegligible rates in both directions. (Note that one can gain an understanding of the situation by assuming that R3 and R161 are in partial equilibrium, whence an expression for the amount of change induced in computed [HNO] induced by the revised heat of formation can be derived analytically. This assumption is only roughly correct over the range of conditions of interest. However, the concentration change predicted in this way is about a factor of two. We have not attempted to determine whether an assumption of partial equilibrium for these reactions could be successfully used as part of a reduced dark zone model.) Thus, because the rate coefficients of back reactions are computed from the thermodynamics, the heat of formation of all of the species involved affects the computed [HNO]. The change in heat of formation causes the computed [HNO] to decrease by about a factor of two; thus, to keep the rate of R19 the same vs the $H_2$/NO kinetics data, k19 (the rate coefficient of R19) must be increased a factor of two. [Note that this factor was found to apply uniformly over the entire range of experiments performed or quoted in Ref. 18. M. C. Lin, in a private communication, has cautioned that an increase by a factor of two in the rate coefficient of R19 makes agreement with the transition state theory calculations of the rate coefficient (Ref. 18 and references therein) somewhat tenuous at the high-temperature end of the range studied (900–1430 K). Typically, one currently expects the best work to result in agreement within a factor of about three, but our proposed two-times increase leads to agreement only within a factor of five. Lin pointed out this suggests there might be some moderately important radical source reaction missing from the mechanism. We agree that this might be the case, but it might also be that our increased rate coefficient is correct and the agreement is simply a little worse than usually obtained in such comparisons. Or, perhaps, the calculated constant needs to be revisited. Until such a reaction or reactions are found, we suggest using our updated k19 in conjunction with the revised HNO heat of formation.] We recommend using the revised HNO heat of formation because this may influence other reactions as well; this forces use of the increased k19. R19 is an important radical source for propellant dark zones, especially for nitrate esters. We find that using the Diau et al.[18] value for k19 increases the predicted nitrate ester dark zone lengths by about a factor of two from those given subsequently (Sec. VIII) and, thus, does not agree well with experiment.

## VII. Burning-Rate Predictions

The primary objective of CYCLOPS is to predict the burning rate of a propellant as a function of its ingredients. Emphasis here is on the word predict. Although our choice of condensed-phase decomposition-product set for a given ingredient may be influenced by the best agreement with the experimental burning rates for that pure ingredient, once determined the decomposition products for each ingredient are considered fixed for purposes of computing burning rates for all of the propellants that include that ingredient. Under these constraints and in the face of the considerable uncertainties associated with the legion input parameters, agreement between the predicted and experimental burning rates should be judged successful if they are within a factor of two.

To illustrate the application of the model to nitrate-ester propellants, calculations were performed on a set of four standard U. S. Army gun propellants including single-base, DB, and triple-base propellants. Thus far, we have not attempted to include minor ingredients such as stabilizers; thus, the nominal formulations are renormalized to reflect these small omissions. The nominal and code-assumed formulations are given in Table 1.

The results for the single-base propellant M10 are shown in Fig. 5. M10, with an average number of $NO_2$ groups of 2.64, is chosen as our prototype for cellulose trinitrate; it has the highest nitration level (13.1%N) of any nearly pure NC (98% NC) for which we had burning-rate data. Two of the three sets of burning rate measurements (Ref. 20 and unpublished data of M. S. Miller, U.S. Army Research Laboratory, Aberdeen Proving Ground, Maryland, 1985–1993) were performed with the same single-batch lot of M10 propellant; the third set of measurements[21] is very consistent with the first two. The CYCLOPS code results are in excellent agreement with these data, even to include the gentle inflection evident at about 10 MPa.

To address DB propellants (and JA2), one needs to have NG and DEGDN in the ingredient database. In previous work,[2] we found a set of decomposition products for NG that worked well to reproduce the burning rates for the gas-phase reaction mechanism then in use. Since that time, we have improved and updated the reaction mechanism and found that the former best decomposition products failed to give satisfactory burning rates with the new mechanism. This illustrates some of our cautionary remarks in the earlier ingredient database discussion. A new best set was found and is used in this work. Of course, there is no guarantee that further improvements to the reaction mechanism, itself a work in progress, will not necessitate new sets of ingredient decomposition products. However, the process should ultimately converge to a single best set limit. These

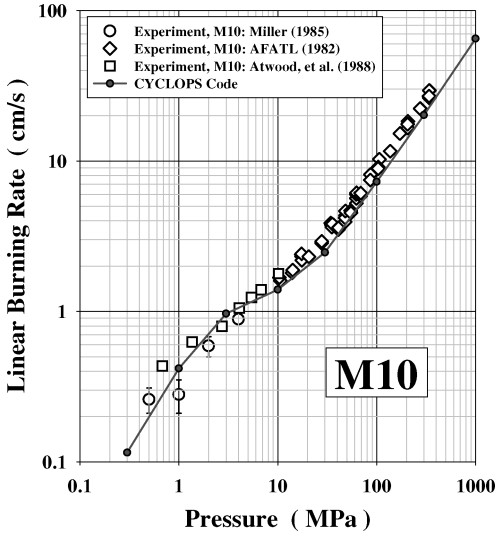


**Fig. 5 CYCLOPS-computed burning-rate pressure dependence for M10 compared to experiments (Refs. 20 and 21 and Miller unpublished data) at 294-K initial temperature.**

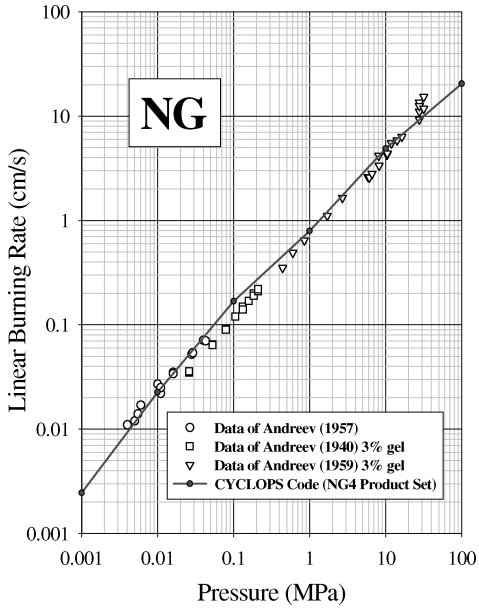


**Fig. 6 CYCLOPS-computed burning-rate pressure dependence for NG using the NG4 product set compared with experiments.[22–24]**

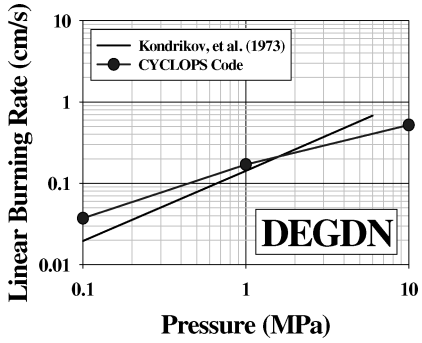


**Fig. 7 CYCLOPS-computed burning-rate pressure dependence for DEGDN compared with experimental data of Kondrikov et al.[25]**

new products for NG are given in Appendix A, and the computed burning rates for NG based on them are shown in Fig. 6 compared to the experimental work of Andreev[22,23] and Andreev et al.[24]

The computed rates are in very good agreement with the measurements over four decades of pressure. The burning rates using the best decomposition products we could find for DEGDN are shown in Fig. 7 along with experimental data.[25] Improvements may well be possible for this ingredient; however, results for JA2 (given later) suggest that the present level of accuracy in the DEGDN product set is probably adequate.

DB propellants of widely varying compositions are shown in Figs. 8–10. M2 propellant (Fig. 8) has a relatively low NG content, M9 (Fig. 9) has a relatively high NG content, and JA2 (Fig. 10) is similar to M9 but with a substantial amount of the NG replaced by DEGDN. Predictions are within a factor of two of the M2 data of Grollman and Nelson,[26] the M9 data of Vanderhoff et al.,[27] the Radford U.S. Army Ammunition Plant's propellant description document,[28] the JA2 data of Miller (unpublished data) and the JA2 data of Juhasz et al.[29]

One aspect of the burning-rate calculations that proved to be a surprise is the sensitivity of the burning rate to small changes in the heats of formation of the ingredients. This sensitivity is a function of pressure, being small at high pressures and sometimes quite large at low pressures. An example of this sensitivity is shown in Fig. 9, where the effects on the computed burning rates of increasing (and decreasing) the heats of formation of all of the ingredients by 3% are illustrated. This computational ability might be used to determine the acceptable tolerances of ingredient purity with respect to the

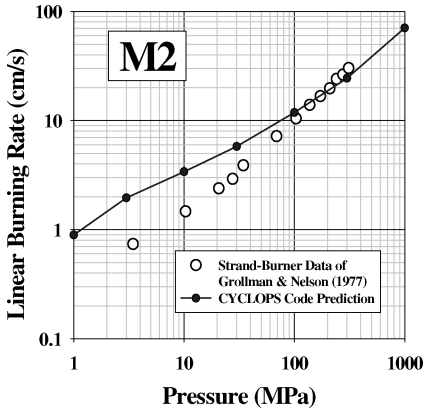


**Fig. 8 CYCLOPS code prediction of M2 burning-rate pressure dependence compared to experiment[26] at 294-K initial temperature.**

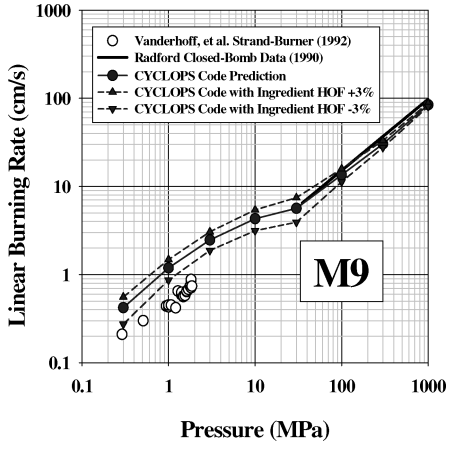


**Fig. 9 CYCLOPS code prediction of M9 burning-rate pressure dependence compared to experiments[27,28] at 294-K initial temperature.**

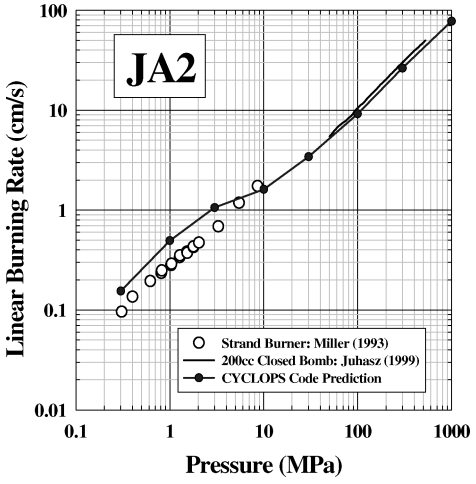


**Fig. 10 CYCLOPS code prediction of JA2 burning-rate pressure dependence compared to experiment (Ref. 29 and Miller unpublished data) at an initial temperature of 294 K.**

burning rate. For example, one could quantitatively determine how much glycerol dinitrate (with its lower heat of formation) could be tolerated in the NG feedstocks.

A final illustration of burning-rate computations with the CYCLOPS code involves the sensitivity of the burning rate to the initial temperature of the propellant. It is worth asking whether Zenin's pyrolysis law[3] retains its universal character for burning rates at different initial temperatures as well as pressures. Figure 11 shows the pyrolysis law data for many different DB formulations along with a

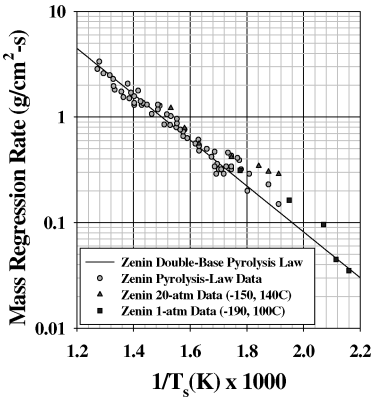


**Fig. 11 Applicability of Zenin's pyrolysis law[3] to DB propellants for extreme initial propellant temperatures.[30]**

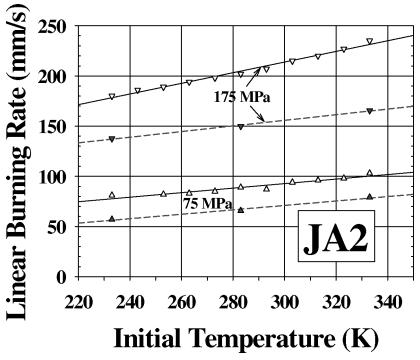


**Fig. 12 Computed initial-temperature dependence of the burning rate of JA2 at 75 and 175 MPa (solid symbols, dashed line linear least-squares fit) compared to the data of Eisenreich et al.[31] (open symbols, solid line linear least-squares fit).**

few data[30] at 1 and 20 atm over a wide range of initial temperatures. The fitted line does not include these initial temperature data; however, it is clear that the wide initial-temperature data are reasonably consistent with the ambient-temperature data, justifying our use of the ambient-temperature pyrolysis law at nonambient temperatures. Eisenreich et al.[31] published measurements of the temperature sensitivity of JA2 burning rates at a number of pressures from 75 to 175 MPa. A comparison of our calculations with their data at the two pressure extremes is shown in Fig. 12. The slopes of the predicted and experimental curves, that is, the change of burning rate for a given change in initial temperature, are fairly close. On the other hand, a commonly used measure is the temperature sensitivity at constant pressure, defined as

$$\sigma_p \equiv \frac{1}{r}\left(\frac{\partial r}{\partial T_0}\right)_p$$

If one were to compare $\sigma_p$, the agreement would not be as good because this quantity is biased by inaccuracies in the magnitude of the burning rate itself.

## VIII. Flame-Structure Predictions

Almost a decade ago Vanderhoff et al.[27] published measurements of gas-phase spatial profiles of temperatures and absolute NO mole fractions for several U.S. Army propellants, including M9 and JA2. These temperature profiles are compared to the predictions of the CYCLOPS code for JA2 at 1.6 MPa in Fig. 13 and for M9 at 1.7 MPa in Fig. 14. Note that both the magnitude of the dark zone temperature and the position of the rapid temperature rise associated with the visible (secondary) flame are very well predicted. The NO mole-fraction profile is also very well predicted for JA2, as shown in Fig. 15. The maximum mole fraction of NO is underpredicted for M9 (Fig. 16) by about 25%, although the agreement for the position of rapid dropoff is good. In Figs. 14 and 16, dashed curves illustrate how the theoretical profiles change if the measured burning rate instead of the computed burning rate is used as input. This was done

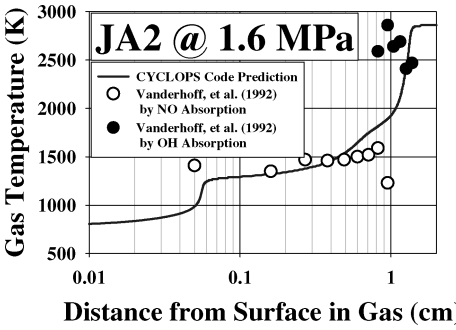


**Fig. 13 Thermal flame-structure predictions of CYCLOPS code for JA2 at 1.6 MPa and 294-K initial temperature compared to experiment.[27]**

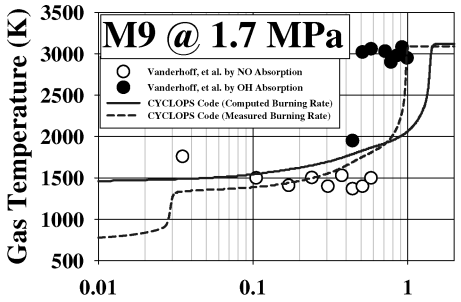


**Fig. 14 Flame-structure predictions of CYCLOPS for M9 at 1.7 MPa and 294-K initial temperature compared to experiment[27]: – – –, temperature profile computed using the measured burning rate instead of the calculated burning rate as input.**

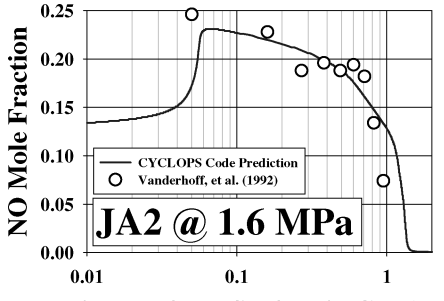


**Fig. 15 NO profile prediction by CYCLOPS for JA2 at 1.6 MPa and 294-K initial temperature compared to experiment.[27]**

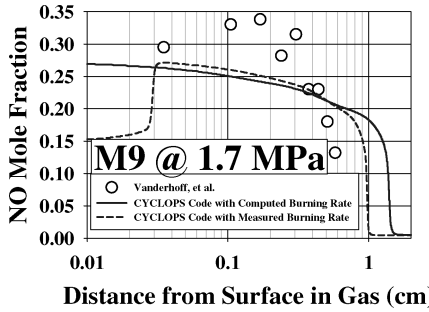


**Fig. 16 NO profile predictions by CYCLOPS for M9 at 1.7 MPa and 294-K initial temperature compared to experiment[27]: – – –, NO profile computed using the measured burning rate as input instead of the calculated burning rate as input.**

**Table 4 Comparison of measured DZ temperatures and mole percents for DB propellants similar to M9 to those computed by CYCLOPS for M9[a]**

| Parameters | Heller and Gordon (1955) | Lengelle et al. (1984) | Vanderhoff et al. (1991) | CYCLOPS (present calculation) |
|---|---|---|---|---|
| $P$, MPa | 1.6 | 0.9 | 1.6 | 1.7 |
| $T_{DZ}$, K | 1600 | 1500 | 1500 | 1543 |
| NO, % | 24 | 21 | 24 | 25 |
| CO | 33 | 38 | | 32 |
| $H_2$ | 8 | 8 | | 8 |
| $N_2$ | 4 | 2 | | 0.4 |
| $H_2O$ | 20 | 20 | | 19 |
| $CO_2$ | 10 | 9 | | 10 |
| HCN | 0.4 | | | 0.4 |
| $CH_4$ | 0.8 | 2.6 | | 0.9 |
| $C_2H_4$ | 0.8 | 0.8 | | 0.1 |

[a]CYCLOPS values taken at 0.1 cm; experimental values and references taken from Vanderhoff et al.[14]

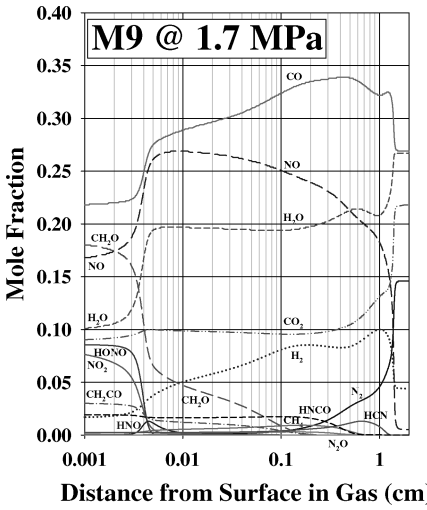


**Fig. 17 Major gas-phase species profiles predicted by the CYCLOPS code for M9 at 1.7 MPa and 294-K initial temperature.**

only in Figs. 14 and 16 to see how strongly the difference between measured and computed burning rate affects the agreement between theory and experiment. It is evident that much of the disagreement can be attributed to inaccuracies in the burning-rate calculation and less to the reaction mechanism. Another useful comparison is between the previous measurements of the chemical species in the dark zone of DB propellants and those predicted by the code. Table 4 has been abstracted from Vanderhoff et al.[14] with the addition of the CYCLOPS mole fraction predictions. All of the measurements are for a hot DB propellant, that is, one with high NG content, at about the same pressure. The CYCLOPS-computed dark zone mole fractions were all taken at a distance from the surface of 0.1 cm for the comparable M9 propellant. Agreement between predictions for most of the species and their respective mole fractions is outstanding. Note that $N_2$ is the only species for which a significant difference occurs. The predictions (Fig. 17), indicate $N_2$ rises to about 3 mole % halfway through the dark zone. The measurements may be more representative of conditions at this point, so that even the agreement for $N_2$ is good. Thus, it appears that the model gives a very credible account of the gas-phase processes, at least insofar as we have been able to test it.

It is of interest to examine the major gas-phase species profiles for several of the propellants studied. Figure 18 shows the major species profiles for JA2 at 1.6 MPa and Fig. 17 the corresponding case for M9 at close to the same pressure on the same scale.

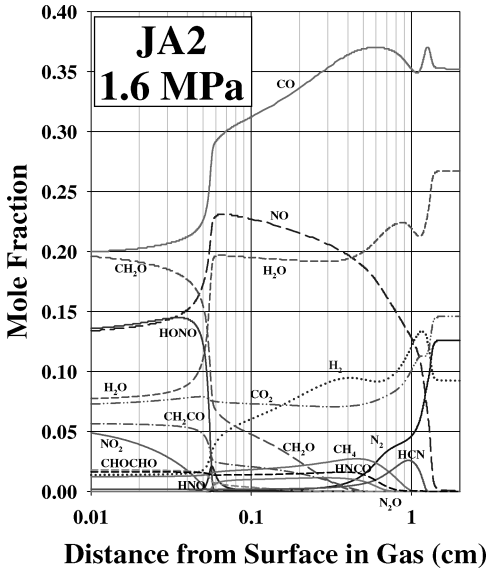


**Fig. 18 Major gas-phase species profiles predicted by the CYCLOPS code for JA2 at 1.6 MPa and 294-K initial temperature.**

## IX. Investigations of the Detailed Gas-Phase Chemistry

It is of interest to determine how the detailed chemistry has led to the predictions of CYCLOPS. This could lend insight, for example, into what types of ingredients might be used to affect the burn rates in some desired manner. As a crucial aid in this effort, we use postprocessing codes written over about the last 10 years for use with PREMIX, namely, PREAD, ChemPlot, and Elemap.[32–34] These codes provide 1) an American Standard Code for Information Interchange (ASCII) output file of many types of information including physical information (heat capacity, heat release rates, density, average molecular weight) and chemical information (sorted rates and sensitivities of individual species and temperature to the various reactions and a pathways table that quickly shows the species reactive flow for a chosen element), 2) the ability to obtain quickly plots of a large variety of information, including the solution variables (species and temperature profiles), and 3) the ability to obtain very rapidly a pathways diagram. The codes have been invaluable in providing the understanding presented herein. As examples, we present details of how a slight inflection in the burning rate vs pressure plot for M10 arises from changes in the key steps in the near-surface gas-phase chemistry, and we discuss and compare the dark zone chemistry for two of the propellants. These examples barely begin the investigations that could be done.

### A. M10 Burning-Rate Pressure Dependence

Although the inflection in the M10 burning-rate curve near 10 MPa is only rather slight, the fact that the experimental and predicted results agree so well suggests that it is real (Fig. 5). It would be of value to determine what consequences such an inflection might have on interior-ballistic calculations beyond those based on the usual simple fit to the $r = aP^n$ law. It is of immense interest to understand nonlinear burning-rate plots such as this. For example, the inflection hints of the beginnings of a plateau region. For certain applications, as in rockets, it can be desirable to obtain long plateau regions because they can reduce the pressure dependence and, thus, the possibility of pressure-induced oscillations.

We have carefully considered the inputs concerned in the present calculations. It is difficult to imagine that anything but variations in the key reactions in the gas-phase chemistry causes the modeling inflection because all of the other inputs vary more smoothly vs pressure. The most important influence on the burning rate at any given pressure is the temperature profile (gradient and absolute value) just above the propellant surface. We have, from our PREAD postprocessing code, the capability of determining the reactions that have

the greatest influence on the temperature just above the surface via sorting of the sensitivities computed using PREMIX. To that end, we present the temperature sensitivities for M10 at the second grid point, that is, the PREMIX-selected grid point just above the surface, for each of the selected pressures in Fig. 5. The value of the temperature at this point, $T_2$, coupled with the surface temperature, is the most sensitive determinant of the computed heat feedback to the surface. Here, we present logarithmically normalized sensitivities, namely,

$$S_k = \frac{A_k}{T_m}\left(\frac{\partial T}{\partial A_k}\right)$$

$T_m$ is the maximum temperature in the calculational domain. Note that $T_m$ is a constant value (usually not the adiabatic temperature, because, to obtain accurate burning rates, the calculational domain may generally be cut off well below the point where that is reached), and multiplication by $A_k$ places the sensitivities on the same relative scale so that the influence of the various reactions can be compared. The sensitivities for the eight pressures are given in Appendix C. Along with the normalized sensitivities, we also present in the last column the value relative to the largest sensitivity for easy comparison. The lists are terminated at the top 20 sensitivity values or at the 5% level. For a given reaction, a positive sensitivity means an increase in the rate coefficient would result in an increase in $T$ near the propellant surface, whereas a negative sensitivity means the opposite. Because the gradient in $T$ would also increase for a positive sensitivity, and vice versa, it is to be expected that a positive sensitivity means an increase in the rate coefficient would generally cause an increase in computed burning rate and vice versa. Note that the reactions listed in Appendix C may have net rates in either direction; these net rates can even reverse at different points in the flame. Most of the reactions that appear in these lists have a noticeably high standing in the sorted rates lists for the species involved (not shown).

A few important points are noted in perusing the sensitivity tables preliminary to pointing out how the changing chemistry vs pressure produces the inflection. First, many of the reactions highest in the lists, that is, most important to determining the heat feedback, involve radical species assumed to be produced in the surface products. Of these radical reactions, many are recombinations that release a lot of heat. An example is R358, $CH_2CO\,(+M) = CH_2 + CO\,(+M)$, which is nearly 100% reversed. These are the primary chemical drivers of the heat into the propellant surface. Some of them, for example, R347, $HCO + NO_2 = CO + HONO$, and R348, $HCO + NO_2 = H + CO_2 + NO$, proceed in the forward direction, indicating two different product sets for the same reactants. This particular pair of reactions is high on the sensitivity lists and with opposite signs probably because R348 is radical neutral, whereas R347 destroys a radical chain-carrying center.

At the lowest pressures, for example, the 0.3-MPa table, we note $T_2$ is primarily influenced by R348, R358, R197, R333, R347, etc. R3, the three-body reaction $H + NO\,(+M) = HNO\,(+M)$ whose rate is highly pressure dependent, is fairly far down the list. As the pressure increases to about 3–10 MPa, the rate of R3 increases faster, relative to the bimolecular reactions, and so it is not surprising that its sensitivity also climbs higher on the sorted list at these pressures. Either R21, $HNO + NO_2 = HONO + NO$, or R161, $H + HNO = H_2 + NO$, rapidly follow R3, so that the sequence of R3 followed by R21 or R161 leads to a modest radical loss. R21 and R161 are very fast and not rate determining in this sequence, which explains why R3 is higher on the sensitivity list. We believe this is why the slope in the burning-rate curve decreases.

At 30 MPa, R19, $HNO + NO = N_2O + OH$, and R166, $HNO + HNO = N_2O + H_2O$, first begin to make their presence in the mechanism known near the surface. Their influence, especially that of R19, increases with increasing pressure until at 1000 MPa R19 is at the top of the list. It is likely these reactions grow in importance because higher pressure causes R3 increasingly to favor a larger [HNO], and for R19, which has a fairly large activation energy of 29 kcal/mole, the higher temperatures observed near the surface as the pressure increases (not shown) will cause the rate of the reaction to greatly increase. Thus, the sensitivity lists indicate these reactions cause the gradient in the burning-rate curve to increase at pressures above 30 MPa.

The strong influence of R19 and R166 on the combustion at pressures above 30 MPa is one of the greatest surprises in this work. Strong evidence has been given in prior works establishing that these reactions are of central importance in controlling the structure (length) of nitrate-ester-propellant dark zones, especially R19, which is the primary radical source that causes the rather dormant mixture to reignite and the secondary flame to form.[14–17] At pressures of 10 MPa and lower, this reaction has a negligible rate near the propellant surface. As the pressure increases, we find that the secondary flame, not surprisingly, moves closer to the propellant surface (not shown). At the highest pressures, there in fact is no dark zone plateau discernable at all in the temperature profile; even so, the dark-zone reactions (R19 and R166) still occur at higher pressures and have a high sensitivity ranking. Detailed analysis shows that the rate of these reactions is negligible very close to the propellant surface, even at 1000 MPa, so that the reason for their high sensitivity rankings is not obvious on that basis.

The physicochemical basis for the increased sensitivity of the burning rate to the dark zone reactions may be further understood by comparing details of the results at two extreme pressures, 1 and 1000 MPa. The concept of characteristic distance for heat transfer in the near-surface region[35] is helpful here. One can express the heat feedback to the surface in terms of the net volumetric heat release from the gas-phase reactions, $q(x)$, by the following simple expression (valid for constant $c_p$ and $\lambda_g$):

$$\lambda_g\left(\frac{\partial T}{\partial x}\right)_{x=0^+} = \int_0^\infty q(x)\exp\left[-\frac{\dot{m}c_p}{\lambda_g}x\right]\mathrm{d}x$$

This expression shows that the heat released at some distance $x$ from the surface contributes to the total heat feedback with exponentially diminshing effectiveness the larger $x$ is relative to the characteristic distance, $\lambda_g/\dot{m}c_p$. We have computed the characteristic distances for the M10 flames to be about $5.5 \times 10^{-4}$ cm at 1 MPa and $8.6 \times 10^{-6}$ cm at 1000 MPa. Temperature and mole-fraction plots for a few key species are given in Figs. 19 and 20. The key feature to look for in these profiles is the distance at which the NO mole fraction peaks, signaling the end of the first reaction stage involving $NO_2$ and HONO reduction. At 1 MPa (Fig. 19), there is subsequently a delay in the reduction of NO to final product $N_2$. This delay is the primary reason for the formation of the dark zone, indicated by the various profiles to be in the region from 0.15 to 1 or 2 cm. The end of the first stage clearly occurs at about 0.15 cm, which is very large compared to the characteristic distance. Thus, the visible flame reactions, which succeed the dark zone reactions, play no role in the heat feedback at this pressure. (Note that the dark zone flame structure and chemistry in the case of M10 at 1 MPa is very similar to that of JA2 at 1.6 MPa, including similar concentrations of trace carbon-containing species and the hump in some of the profiles at midpoint of the dark zone, except that the dark zone

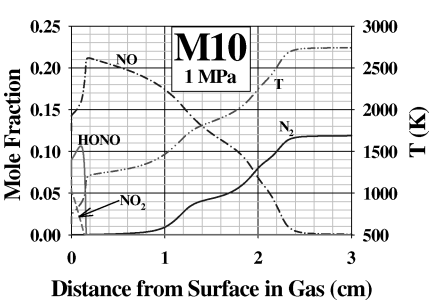


**Fig. 19 Key species profiles defining the DZ along with the temperature profile for M10 at 1 MPa.**

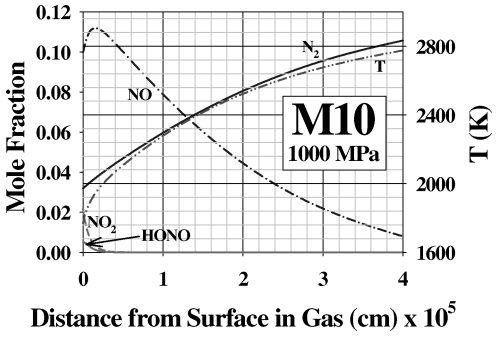


**Fig. 20 Key species profiles defining the DZ along with the temperature profile for M10 at 1000 MPa.**

is, not surprisingly, longer at this lower pressure. The chemistry of the JA2 dark zone is considered in more detail and compared with M9 in the next section.) At 1000 MPa (Fig. 20), the profiles do not indicate the existence of a separate dark zone region because, in this case, the dark zone reactions are greatly accelerated due to the higher temperature and pressure. Thus, the dark zone reactions no longer act as a slow, spatially extended bottleneck for creating the radicals responsible for releasing the heat of the visible flame. Because at this pressure the characteristic distance is larger than the distance at which the NO begins to disappear, some of the energy release associated with the visible flame contributes to the heat feedback. This explains the high sensitivity rankings of R19 and R166 (and also R341, R181, and R149, which are associated with trace dark zone species).

It previously had been thought by most workers (including the authors) that the chemistry responsible for the formation of dark zones at low pressure cannot affect the burning rates of propellants. This belief was based on the argument that, at low pressures, this chemistry keeps the secondary-flame energy release remote from the surface, and at high pressures, the dark zones are not perceptible in photographs, presumably meaning that the dark-zone chemistry is no longer relevant. *Our analysis of the reactions critically determining the high-pressure burning rate show that this chain of reasoning is, in fact, wrong. The reactions causing the formation of dark zones at low pressure are extremely important to the burning rate at high pressure*. Because this chemistry has not been very well established, especially for nitramine propellants, it is important for it to receive renewed attention.

### B. Dark Zone Structure in JA2 and M9

One of the more curious features often observed in the flame structures of combusting propellants at low pressure (less than approximately 100 atm) is the formation of a dark zone (DZ), a nonluminous region between the condensed-phase propellant and the high-temperature luminous flame zone. The discussion on M10 in the last section indicates DZ chemistry may become extremely important to the propellant burning rate at high pressures. The chemistry of this feature is also of technical interest in its own right. Therefore, the DZ chemistry observed in this work is discussed here in more detail.

As noted in the earlier discussion of flame structure, our computations at about 1–2 MPa predict the formation of DZs for JA2, M9, and M10. (Computations for M2 were not performed at large distances; it undoubtedly also does form a DZ.) This result is evidenced by the appearance of near-plateau regions in the various concentration and temperature profiles. For example, for JA2, from the temperature profile in Fig. 13, the DZ at 1.6 MPa extends from the end of the first-stage combustion, 0.055 cm to about 1.3 cm, where the sharp upward temperature gradient indicates that the runaway in the second-stage chemistry to final equilibrium occurs. It is well known in the case of nitrate-ester propellants that DZs form because of the conversion of $NO_2$ and HONO near the propellant surface to NO and that the intermediate NO is a slowly reacting oxidizer that retards the chemistry.[14–17] The end of the DZ, signified by rapid conversion of the intermediates to final products with a rapid temperature rise, occurs due to the buildup of heat and, especially, radical concentrations. Though the DZ was intriguing to early researchers, its existence can be simply explained as the result of a delayed chemical ignition of the second reaction stage due to the presence of comparatively unreactive intermediates. (NO is the unreactive intermediate in the case of nitrate-ester propellants and NO and HCN in the case of nitramine propellants. Note that ignition delays in chemistry on formation of a hot gaseous mixture are not at all unusual; they are frequently observed, especially in shock tube experiments. The challenge in the case of propellants is to determine the correct chemistry for a rather complicated mixture with rather scant experimental information available about the exact conditions at leading edge of the DZ.) The primary constituents of the DZ for nitrate-esters are $H_2$, NO, CO, $CO_2$, $N_2$, and $H_2O$ (Figs. 17 and 18 and Table 4). In general, the concentrations of the first three species are above equilibrium values, whereas the latter three are below. At the runaway point, conversion of the first three to final products occurs. A simplified kinetic scheme[14,16,17] indicates that R19, $HNO + NO = N_2O + OH$, is the primary source reaction for radical buildup in the case of nitrate-esters. Thus, the DZ length is quite sensitive to the rate coefficient chosen for R19. At the end of the DZ, where the final steep temperature gradient occurs, the remaining NO is converted to final product $N_2$, mostly via R165, $NO + H = N + OH$, followed rapidly by R163, $N + NO = N_2 + O$; some of the CO is converted to $CO_2$ via R44, $CO + OH = CO_2 + H$, and some of the $H_2$ is converted to $H_2O$ via R52, $O + H_2 = OH + H$, followed by R50, $OH + H_2 = H_2O + H$.

One feature in common to the temperature profiles that is surprising is the presence of a slight hump about halfway through the DZ. These humps are most prominent in the 1.6-MPa JA2 profile at 0.7 cm (Fig. 13) and the 1.0-MPa M10 profile at 1.3 cm (Fig. 19). There is a more modest one in the 1.7-MPa M9 profile at 0.5 cm (Fig. 14). Such a hump is not readily discerned in most experimental profiles; it is a rather small feature that would not be easy to observe. Example figures and photographs of burning propellants given in the literature and presentations frequently have been carefully chosen to illustrate the qualitative features of the phenomenon, especially the DZ. What is frequently not pointed out in various still-picture examples is that there is almost always a fairly large amount of flicker in the flame position. This may have contributed to the overlap in temperature regions at the end of the JA2 and M9 DZs in the experimental results of Figs. 13 and 14. The measurements were made using absorption spectroscopy on NO and OH, which are primarily present in the intermediate- (DZ) temperature and high-temperature spatial regions, respectively. The measurements indicate the intermediate temperatures extend to about 0.2 cm larger distances than those at which the high temperatures begin. The problem with flickering can also be compounded with reproducibility and spatial resolution difficulties. (The NO and OH results were from different runs.) Thus, the lack of a hump in experimental profiles cannot necessarily be taken as evidence against the present prediction of a modest hump. Evidence for the presence of such a hump is found in the temperature profile taken at 5.0 MPa for the DB propellant N-powder in the work of Zenin.[36]

Because the major reactions controlling the DZ behavior were already discussed in the last paragraph, in the remainder of this section we discuss the predicted chemistry of the trace DZ species and compare the results for JA2 and M9. (Although the modeling was done at slightly different pressures, taken to match the available experiments, these are close enough to make comparisons reasonable.) Note that, as we will discuss further later, the hump primarily arises from reactions of trace species that are present at the leading edge of the DZ. One could have a concern here that some of the trace species predicted are the result of our assumed condensed-phase products for the various ingredients and that these may not be unique. In other words, the question arises whether the entire idea may be incorrect and the effort here to investigate the associated chemistry is wasted. However, predicted and observed DZ-species concentrations (Table 4) are quite close even for most of the trace species. These similarities, especially that of $CH_4$, which we will see

is very important in this discussion, suggest the associated chemistry and predicted consequences to the temperature profile are at least qualitatively correct.

Intermediate trace species predicted in the DZs of JA2 at 1.7 MPa and M9 at 1.6 MPa include $CH_4$, HCN, HNCO, $N_2O$, HNO, $CH_2O$, and $CH_2CO$, as well as HCNO. The first seven of these are shown in Figs. 17 and 18 and are present at the level of several mole percent. The species $CH_2O$ and $CH_2CO$ are the primary fuels in the first stage. $CH_2CO$ is formed near the surface, primarily from the rapid recombination of $CH_2$ with CO (−R358), whereas $CH_2O$ is present as a condensed-phase product. In the first stage, most of the $CH_2O$ and $CH_2CO$ react, globally, with $NO_2$ and HONO oxidizers, yielding $H_2$, $H_2O$, CO, and the less reactive NO oxidizer. A few percent of the $CH_2O$ and $CH_2CO$ fuels remains from this rich mixture. $CH_4$ comes from the condensed phase (Table 3), and is formed early in the first stage via R310, $CH_3 + CH_2O = CH_4 + HCO$, and early in the DZ by −R222, $CH_3 + H_2 = H + CH_4$. Note that the $CH_3$ formed early in the DZ arises from consumption of part of the leftover $CH_2CO$ via R365, $CH_2CO + H = CH_3 + CO$. Thus, all of $CH_2$, $CH_3$, and $CH_4$ coming from the condensed phase can directly or indirectly contribute to $CH_4$ observed in the DZ.

Note that at the point of the sharp gradients dividing the first and second stages (0.055 cm for JA2 and 0.0045 cm for M9) there is a sudden, sharp peaking in the concentration of HNO to about 1 or 2 mol%. HNO is formed at this point primarily by R197, $HCO + NO = HNO + CO$. However, we have been unable to discern why the HNO profile is so strongly peaked and what controls its maximum concentration. The HNO concentration apparently controls the amount of trace $N_2O$ formed at the leading edge of the DZ. $N_2O$ is formed here as the HNO is consumed, primarily via R166, $HNO + HNO = N_2O + H_2O$. (We have found that the relative concentration of $N_2O$ in M9 vs JA2 DZs is roughly proportional to the square of the [HNO]. R166 is second order in HNO, and the temperature difference between the two propellants at the end of the first stage is small, which suggests such a proportionality is to be expected.) A small portion of the $N_2O$ formed at this point is due to R19, $HNO + NO = N_2O + OH$. R19 is also primarily responsible for the slight continuation of growth in $[N_2O]$ until its maximum partway through the DZ.

Traces of HCNO and HNCO are formed primarily early in the first stage via reactions of $CH_2$ with NO (R335 and R333, respectively). HCNO is converted to HNCO early in the DZ via R341, $HCNO + H = H + HNCO$, accounting for the slight increase in HNCO to its maximum value about midway through the DZ. At the same time as the HCNO is being consumed, the leftover traces of $CH_2O$ are converted to CO and $H_2$. The leftover traces of $CH_2CO$ are converted to CO, $CH_2$, and $CH_3$ via unimolecular reaction R358 and reaction with H atom, R365. As already mentioned, the $CH_3$ is rapidly converted temporarily to $CH_4$ via reaction with $H_2$ (−R222) and is one of the primary sources of the $CH_4$ in the DZ. The $CH_2$ rapidly reacts with NO to make more HNCO via R333.

After the consumption of $CH_2O$, $CH_2CO$, and HCNO, the $CH_4$, HNCO, and $N_2O$ almost simultaneously begin to be consumed. This concerted process is the main source of the heat release and the hump in the temperature profiles about midway through the DZs. Pathway diagrams for JA2 illustrate the chemical pathways connecting nitrogen- and carbon-containing species in this spatial region (Fig. 21, based on relative rates of the chemical reactions integrated over the spatial coordinate from 0.5 to 0.75 cm, resulting in units of mole per square centimeter per second before the normalization to 100). Consumption of $CH_4$ occurs primarily via H atom abstraction reactions with H and OH (R222 and R257) to form $CH_3$. R339, $CH_3 + NO = HCN + H_2O$, then rapidly occurs, as well as secondary reaction R340, temporarily forming $H_2CN$. HCN is a relatively stable intermediate because both bonds are strong. (Its C–H bond is, for example, about 20 kcal/mol stronger than the C–H bond in $CH_4$.) Like much of the NO, most of it, therefore, survives to the end of the DZ. HNCO reacts primarily via R181, $HNCO + H = NH_2 + CO$; some is diverted in a secondary path to NCO. The $NH_2$ thus formed rapidly reacts with NO: R149, $NH_2 + NO = N_2 + H + OH$, and R150, $NH_2 + NO = N_2 + H_2O$. (In

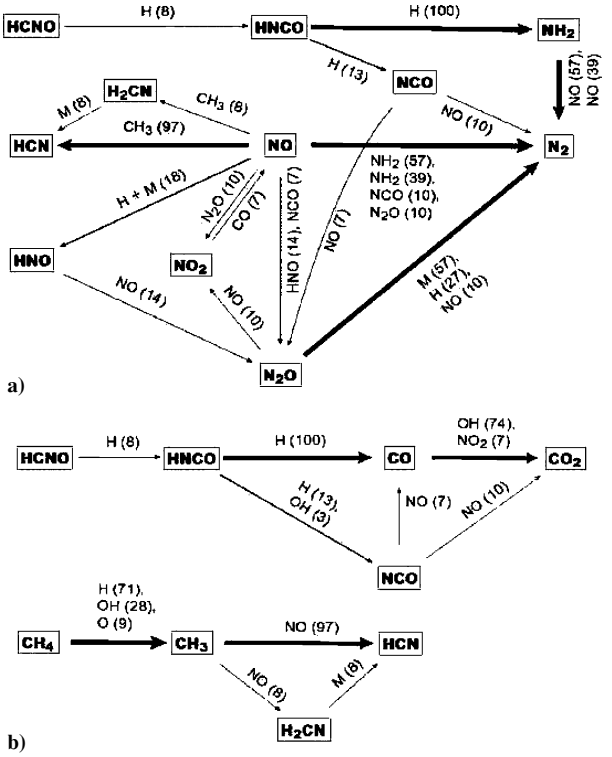


**Fig. 21 Pathway diagrams for chemistry of JA2 at 1.6 MPa in the region leading up to the hump in the DZ temperature profile at about 0.7 cm; relative integrated (over 0.5 to 0.75 cm) rate of 100 is 4.99 × $10^{-4}$ mol/cm$^2$ · s (reaction of HNCO with H in both cases): a) nitrogen species and b) carbon species.**

Fig. 21a nitrogen pathways, R149 is the one that is modestly faster.) $N_2O$ is primarily consumed by R2, $N_2O$ (+M) = $N_2$ + O (+M), and R113, $N_2O + H = N_2 + OH$. (Note that R149 and R2, as well as R19, can contribute to radical buildup.) For JA2, the sorted heat releases indicate the primary exothermic reactions in this region are, in decreasing order of importance, R339, R150, and R113. These are slightly countered by the endothermic R2, whose heat consumption is roughly equivalent to the heat production of R113. For M9, similar analysis indicates R150 and R339 are, in order, the most important. (Although these reactions account for the bulk of the heat release, there are several other reactions whose heat releases are up to about half the size of the smallest of these.) Pathway diagrams (not shown) in the region leading up to the M9 hump are similar to those for JA2, except that $CH_4$, $CH_3$, and $N_2O$ reactions are much less important relative to HNCO reactions.

We are now in a position to explain the relative sizes of the humps in the JA2 and M9 temperature profiles. $CH_4$ and HNCO are the main species whose reactions produce the heat that gives rise to these humps. Thus, $CH_4$ arises 1) directly from the assumption of its production from the condensed phase, 2) from $CH_3$ reaction with $CH_2O$ in the first stage, and 3) from temporary conversion of $CH_2$ in the first stage to $CH_2CO$, followed early in the DZ by the sequence $CH_2CO \rightarrow CH_3 \rightarrow CH_4$. HNCO arises 1) directly from $CH_2$ + NO near the surface and 2) by $CH_2$ + NO production of HCNO near the surface followed by conversion of HCNO to HNCO at the leading edge of the DZ. The trace concentrations of $CH_4$ and HNCO species, which ultimately give rise to the humps in the respective temperature profiles, are larger for JA2 than for M9. Thus, the hump is more pronounced for JA2 than for M9 (Figs. 13 and 14). Finally, the reason concentrations of $CH_4$ and HNCO are larger for JA2 may be understood by perusal of Table 3. The $CH_4$, $CH_3$, and $CH_2$ concentrations, produced from the condensed-phase reactions and which lead to $CH_4$ and HNCO, are all larger for JA2 than for M9. (Similar observations also apply to M10, which produces the relatively pronounced hump in Fig. 19. Although the model assumes no $CH_4$ or $CH_3$ are produced from the condensed phases, there is a relatively large amount of $CH_2$. $CH_2$, as already discussed, can lead

to HNCO and $CH_4$ production in various portions of the flame and their ultimate consumption in the DZ.)

## X. Conclusions

The current state of the art in energetic-material combustion modeling could be described as one of frustrated opportunity. On the one hand, great progress has been made in developing credible elementary reaction mechanisms for the gas phase; on the other hand, progress in describing condensed-phase and surface processes has been far less than commensurate. The approach embodied by the CYCLOPS code takes full advantage of the availability and present possibility of good elementary-reaction gas-phase mechanisms while offering a viable strategy for dealing quantitatively with the unknown mechanics of subsurface reaction and surface regression through the agency of the pyrolysis law. The link between the pyrolysis law of mass regression and the detailed chemistry of the gas phase is effected by hypothesizing the condensed-phase decomposition products in number and kind consistent with atomic balance and available experimental results. Although our present approach is clearly an interim solution waiting for a comprehensive treatment of the burning-surface and condensed-phase processes, there are a number of features in its favor. Burning rate often is not a sensitive function of the underlying submodels. CYCLOPS exploits this insensitivity because small imperfections in the decomposition-product set for any one ingredient may not seriously degrade the calculated burning rate for the whole multi-ingredient propellant.

Another favorable feature of our approach is the generality of its assumptions. The pyrolysis law has been found to provide a good empirical description of both reactive and evaporative surface regression mechanisms. (Evaporative mechanisms for ozone and RDX are discussed in Ref. 2.) The set of decomposition products for each ingredient used in this study may well not be optimum, but they can be easily changed as new research results become available. Apart from the potentially imprecise assumption that the ingredients decompose (in the condensed phase) independently of each other, the approach taken here must work if the combustion is one dimensional, the pyrolysis law is valid, the decomposition products are correct, and the gas-phase reaction mechanism is complete and accurate. Of course, the accuracy of the predicted burning rate will also be a function of the accuracy of other input data, such as the ingredient and propellant-amalgam heats of formation, that even a hypothetically rigorous model would require as well. Thus, CYCLOPS is a flexible vehicle for making practical calculations of the formulation dependence of burning rate while incorporating evolving improvements in mechanistic understanding. Note that the model does not have to be perfect to be useful; it would be enormously helpful to have even semi-quantitatively correct theoretical guidance in propellant-formulation work. Finally, even if molecular-dynamic simulations of the condensed-phase and surface-regression phenomena should become routine and reliable, the calculational model proposed here may well be the most practical way of coupling those results with the present rigorous continuum-mechanics description of the gas phase to predict burning rates.

## Appendix A: Ingredient Database

## Appendix B: Gas-Phase Reaction Mechanism

## Appendix C: Ranked Sensitivity Coefficients for Temperature at First Gas-Phase Grid Point for M10

**Detailed information on the above can be obtained directly from the corresponding author at willie@arl.army.mil.**

## References

[1]Miller, M. S., Rice, B. M., Kotlar, A. J., and Cramer, R. J., "A New Approach to Propellant Formulation: Minimizing Life-Cycle Costs through Science-Based Design," *Clean Products and Processes*, Vol. 2, No. 1, 2000, pp. 37–46.

[2]Miller, M. S., and Anderson, W. R., "Energetic-Material Combustion Modeling with Elementary Gas-Phase Reactions: A Practical Approach," *Solid Propellant Combustion Chemistry, Combustion, and Motor Interior Ballistics*, edited by V. Yang, T. B. Brill, and W. Z. Ren, Vol. 185, Progress in Astronautics and Aeronautics, AIAA, Reston, VA, 2000, Chap. 2.12, pp. 501–531.

[3]Zenin, A., "HMX and RDX: Combustion Mechanism and Influence on Modern Double-Base Propellant Combustion," *Journal of Propulsion and Power*, Vol. 11, No. 4, 1995, pp. 752–758.

[4]Kee, R. J., Grcar, J. F., Smooke, M. D., and Miller, J. A., "A Fortran Program for Modeling Steady Laminar One-Dimensional Premixed Flames," Sandia National Lab., Rept. SAND85-8240, Livermore, CA, Dec. 1985.

[5]Miller, M. S., and Coffee, T. P., "On the Numerical Accuracy of Homogeneous Solid Propellant Combustion Models," *Combustion and Flame*, Vol. 50, No. 1, 1983, pp. 75–88.

[6]Leider, H. R., and Seaton, D. L., "Nitrate Ester Decomposition and Degradation of Molecular Weight in Nitrocellulose from Thermal Decomposition of PBX-9404 below 100C," Lawrence Livermore Lab., Rept. UCRL-52776, Livermore, CA, May 1979.

[7]Gelernter, G., Browning, L. C., Harris, S. R., and Mason, C. M., "The Slow Thermal Decomposition of Cellulose Nitrate," *Journal of Physical Chemistry*, Vol. 60, No. 8, 1956, pp. 1260–1264.

[8]Bunte, S. W., and Miller, M. S., "Atomistic Simulations of the Physical Properties of Nitrate Esters," U.S. Army Research Lab., TR ARL-TR-2496, Aberdeen Proving Ground, MD, May 2001.

[9]Todd, J., and Glasser, W. G., "NMR Spectroscopy of Nitrocellulose Samples," Contract Rept. to AlliantTechSystems, Inc., Radford, VA, Glasser, W. G., and Audrey G. Zink, A. G. "Final Report on Cellulose and Cellulose Nitrate Characterization," Sec. IV, Virginia Polytechnic Inst. and State Univ., Blacksburg, VA, Feb. 1996.

[10]Taylor, J., Hall, C. R. L., and Thomas, H., "The Thermochemistry of Propellant Explosives," *Journal of Physical and Colloid Chemistry*, Vol. 51, No. 2, 1947, pp. 580–592.

[11]Miller, M. S., and Kotlar, A. J., "Thermal Transport Properties of Solid Gun Propellants," *Proceedings of the 29th JANNAF Combustion Subcommittee Meeting*, CPIA Publ. 593, Vol. 1, Chemical Propulsion Information Agency, Columbia, MD, 1992, pp. 149–159.

[12]Vladimiroff, T., Carignan, Y. P., Chiu, D. S., and Macpherson, A. K., "The Development of a User Friendly Thermodynamic Code for the Personal Computer," *24th JANNAF Combustion Meeting*, CPIA Publ. 476, Vol. 2, Chemical Propulsion Information Agency, Columbia, MD, 1987, pp. 39–44.

[13]Vladimiroff, T., Carignan, Y. P., Chiu, D. S., and Macpherson, A. K., "Flame Temperature Calculations at High Temperature and Pressure," *Propellants, Explosives and Pyrotechnics*, Vol. 19, No. 6, 1994, pp. 281–285.

[14]Vanderhoff, J. A., Anderson, W. R., and Kotlar, A. J., " Dark Zone Modeling of Solid Propellant Flames," *Proceedings of the 29th JANNAF Combustion Subcommittee Meeting*, CPIA Publ. 593, Vol. 2, Chemical Propulsion Information Agency, Columbia, MD, 1992, pp. 225–237.

[15]Anderson, W. R., "The Chemical Mechanism of $H_2$/NO Combustion at Intermediate Temperatures and Its Relation to the Dark Zone of Propellants," *30th JANNAF Combustion Subcommittee Meeting*, CPIA Publ. 606, Vol. 2, Chemical Propulsion Information Agency, Columbia, MD, 1993, pp. 205–215.

[16]Anderson, W. R., Ilincic, N., Meagher, N. E., Seshadri, K., and Vanderhoff, J. A., "Detailed and Reduced Chemical Mechanisms for the Dark Zones of Double Base and Nitramine Propellants in the Intermediate Temperature Regime," *Proceedings of the 32nd JANNAF Combustion Subcommittee Meeting and 1995 Propulsion Systems Hazards Subcommittee Meeting*, Joint Sessions, CPIA Publ. 638, Vol. 1, Chemical Propulsion Information Agency, Columbia, MD, 1995, pp. 197–214.

[17]Ilincic, N., Anderson, W. R., Seshadri, K., and Meagher, N. E., "Simplified Chemical–Kinetic Mechanisms for Characterizing the Structure of the Dark Zones of Double Base and Nitramine Propellants," *Twenty-Sixth Symposium (International) on Combustion*, Vol. 2, Combustion Inst., Pittsburgh, PA, 1996, pp. 1997–2006.

[18]Diau, E. W., Halbgewachs, M. J., Smith, A. R., and Lin, M. C., "Thermal Reduction of NO by H2: Kinetic Measurement and Computer Modeling of the HNO + NO Reaction," *International Journal of Chemical Kinetics*, Vol. 27, No. 9, 1995, pp. 867–881.

[19]Anderson, W. R., "Heats of Formation of HNO and Some Related Species," *Combustion and Flame*, Vol. 117, Nos. 1–2, 1999, pp. 394–403.

[20]Juhasz, A. A. (ed.), *Round Robin Results of the Closed Bomb and Strand Burner*, CPIA Publ. 361, Chemical Propulsion Information Agency, Columbia, MD, 1982.

[21]Atwood, A. I., Price, C. F., Curran, P. O., and Zwierzchowshi, N. G., "Burning Rate, Radiant Ignition, and Global Kinetics of a Nitrocellulose Propellant," *25th JANNAF Combustion Meeting*, Publ. 498, Vol. 1, Chemical Propulsion Information Agency, Columbia, MD, 1988, pp. 69–81.

[22]Andreev, K. K., "Experimental Investigation on Combustion of Explosives," *Collection of Articles on Theory of Explosives*, Oborongiz, Moscow, 1940, pp. 39–65.

[23]Andreev, K. K., *Thermal Decomposition and Combustion of Explosives*, Gosenergoizdat, Moscow, 1957.

[24]Andreev, K. K., Glazkova, A. P., and Tereshkin, I. A., "Investigation of Pressure, Temperature, and Density Influence on Combustion, Explosives, and Some Composites," Chemical Physics Inst., Moscow, 1959.

[25]Kondrikov, B. M., Raikova, V. M., and Samsonov, B. S., "Kinetics of Combustion of Nitro-Compounds at High-Pressure," Combustion, Explosion, and Shock Waves, Vol. 9, No. 1, 1973, pp. 68–73.

[26]Grollman, B. B., and Nelson, C. W., "Burning Rates of Standard Army Propellants in Strand Burner and Closed Chamber Tests," U.S. Army Ballistic Research Lab., Memorandum Rept. BRL MR 2775, Aberdeen Proving Ground, MD, Aug. 1977.

[27]Vanderhoff, J. A., Teague, M. W., and Kotlar, A. J., "Absorption Spectroscopy through the Dark Zone of Solid Propellant Flames," U.S. Army Ballistic Research Lab., TR BRL-TR-3334, Aberdeen Proving Grounds, MD, April 1992.

[28]Kirkpatrick, D. W., "Propellant Description Sheet for M9, DA Lot Number RAD-PE-792-77," Radford U.S. Army Ammunition Plant, Radford, VA, April 1990.

[29]Juhasz, A., Bullock, C., Homan, B., and Devynck, D., "Micro Closed Bomb for Characterizing the Burning of Propellants at Gun Pressures," *36th JANNAF Combustion Subcommittee Meeting*, CPIA Publ. 691, Vol. 1, Chemical Propulsion Information Agency, Columbia, MD, 1999, pp. 175–187.

[30]Zenin, A. A., and Nefedova, O. I., "Burning of Ballistite Powder over a Broad Range of Initial Temperatures," Combustion, Explosion, and Shock Waves, Vol. 3, No. 1, 1967, pp. 26–33.

[31]Eisenreich, N., Eckl, W., Fischer, T., Weiser, S., Langer, G., and Baier, A., "Burning Phenomena of the Gun Propellant JA2," *Propellants, Explosives, Pyrotechnics*, Vol. 25, No. 3, 2000, pp. 143–148.

[32]Anderson, W. R., Haga, S. W., Nuzman, J. F., Kotlar, A. J., and Anderson, R. J., "PREAD Computer Code: A Versatile, Portable FORTRAN Computer Code for Interpreting the Complex Chemical Kinetics and Transport Properties of a Premixed, Laminar, Steady-State Flame," U.S. Army Research Lab., Aberdeen Proving Grounds, MD, 1990–2002.

[33]Anderson, R. J., Nuzman, J. F., Anderson, W. R., and Bitely, J. J., "ChemPlot Computer Code: A Portable JAVA Computer Code for Rapid, On-line Visualization of Complex Chemical Kinetic Code Outputs," U.S. Army Research Lab., Aberdeen Proving Grounds, MD, 1997–2002.

[34]Anderson, R. J., and Anderson, W. R., "ELEMAP: An Interactive, Portable, JAVA Computer Code for Rapid Visualization of Chemical Pathways Diagrams Related to Complex Chemical Kinetic Code Outputs," U.S. Army Research Lab., Aberdeen Proving Grounds, 1999–2002.

[35]Miller, M. S., "Three-Phase Combustion Modelling: Frozen Ozone, a Prototype System," *Proceedings of the Materials Research Society Symposium: Decomposition, Combustion and Detonation Chemistry of Energetic Materials*, edited by T. B. Brill, T. P. Russell, W. C. Tao, and R. B. Wardle, Materials Research Sociey, Pittsburgh, PA, 1996, pp. 169–180.

[36]Zenin, A. A., "Structure of Temperature Distribution in Steady-State Burning of a Ballistite Powder," *Fizika Goreniya i Vzryva*, Vol. 2, No. 3, 1966, pp. 67–76.


# Elements of Spacecraft Design

**Charles D. Brown,** *Wren Software, Inc.*

This new book is drawn from the author's years of experience in spacecraft design culminating in his leadership of the Magellan Venus orbiter spacecraft design from concept through launch. The book also benefits from his years of teaching spacecraft design at University of Colorado at Boulder and as a popular home study short course.


The book presents a broad view of the complete spacecraft. The objective is to explain the thought and analysis that go into the creation of a spacecraft with a simplicity and with enough worked examples so that the reader can be self taught if necessary. After studying the book, readers should be able to design a spacecraft, to the phase A level, by themselves.

Everyone who works in or around the spacecraft industry should know this much about the entire machine.

**Table of Contents:**

- ❖ Introduction
- ❖ System Engineering
- ❖ Orbital Mechanics
- ❖ Propulsion
- ❖ Attitude Control
- ❖ Power System
- ❖ Thermal Control
- ❖ Command And Data System
- ❖ Telecommunication
- ❖ Structures
- ❖ Appendix A: Acronyms and Abbreviations
- v Appendix B: Reference Data
- v Index

*AIAA Education Series*

2002, 610 pages, Hardback • ISBN: 1-56347-524-3 • List Price: $111.95 • **AIAA Member Price: $74.95**

American Institute of Aeronautics and Astronautics
Publications Customer Service, P.O. Box 960, Herndon, VA 20172-0960
Fax: 703/661-1501 • Phone: 800/682-2422 • E-mail: warehouse@aiaa.org
**Order 24 hours a day at www.aiaa.org**

AIAA
American Institute of Aeronautics and Astronautics

02-0547